Available online at www.sciencedirect.com
ScienceDirect
Computer Physics Communications 175 (2006) 575–582
Computer Physics Communications
www.elsevier.com/locate/cpc

A model for semiconductor quantum dot molecule based on the current spin density functional theory ☆

Jinn-Liang Liu [a,*], Jen-Hao Chen [b], O. Voskoboynikov [c]

[a] *Department of Applied Mathematics, National University of Kaohsiung, Kaohsiung 811, Taiwan*
[b] *Department of Applied Mathematics, National Chiao Tung University, Hsinchu 300, Taiwan*
[c] *Department of Electronic Engineering, National Chiao Tung University, Hsinchu 300, Taiwan*

Received 29 March 2006; accepted 6 June 2006

Available online 1 September 2006

Abstract

Based on the current spin density functional theory, a theoretical model of three vertically aligned semiconductor quantum dots is proposed and numerically studied. This quantum dot molecule (QDM) model is treated with realistic hard-wall confinement potential and external magnetic field in three-dimensional setting. Using the effective-mass approximation with band nonparabolicity, the many-body Hamiltonian results in a cubic eigenvalue problem from a finite difference discretization. A self-consistent algorithm for solving the Schrödinger–Poisson system by using the Jacobi–Davidson method and GMRES is given to illustrate the Kohn–Sham orbitals and energies of six electrons in the molecule with some magnetic fields. It is shown that the six electrons residing in the central dot at zero magnetic field can be changed to such that each dot contains two electrons with some feasible magnetic field. The Förster–Dexter resonant energy transfer may therefore be generated by two individual QDMs. This may motivate a new paradigm of Fermionic qubits for quantum computing in solid-state systems.

Keywords: Density functional theory; Cubic eigenvalue problem; Jacob–Davidson method

1. Introduction

There is significant interest in quantum information processing based on fermionic qubits using semiconducting materials [1–10]. One of the proposals in this approach is to exploit electronic excitations of coupled quantum dots (QDs) that form an artificial molecule (QDM) [6,7,9,10]. In particular, an energy selective scheme to manipulating excitonic states of QDM, together with control over the Förster–Dexter resonant energy transfer and biexciton binding energy, can be used to perform quantum computation and to produce controlled exciton quantum entanglement [7,11]. The resonant Förster–Dexter energy transfer mechanism is also responsible for photosynthetic energy process in antenna complexes, biosystems that harvest sunlight [12]. It has been recently shown that two individual closely spaced fluorescent molecules undergo a strong coherent dipole–dipole coupling can produce entangled states [13]. We propose and numerically investigate here a theoretical model of three vertically aligned InAs/GaAs QDM whose dimensions are commensurable with that of [9] in which a transmission electron micrograph of a QDM sample is illustrated.

Our QDM model consists of one large central dot and two smaller dots situated above and beneath the central dot whose geometrical dimensions are shown in Fig. 1 where the radius, thickness, and separation of each dot are indicated by coordinates. It has been demonstrated in [11,14] that there exists Förster energy transfer from smaller to larger dots via electrostatic coupling. Our goal for this model system is to investigate the detailed electronic properties of the QDM with $N = 6$ electrons under the effects of an external magnetic field by using the current spin density functional theory (CSDFT) [15,16].

For the many-body Hamiltonian of our QDM model, we extend the models used in [17–19], which are based on parabolic one-band effective-mass envelope function approximation with either infinite or quadratic confinement potentials, to a more

☆ This work was supported by NSC under Grant 94-2115-M-009-009, Taiwan.
* Corresponding author.
E-mail address: jinnliu@nuk.edu.tw (J.-L. Liu).

0010-4655/$ – see front matter
doi:10.1016/j.cpc.2006.06.009

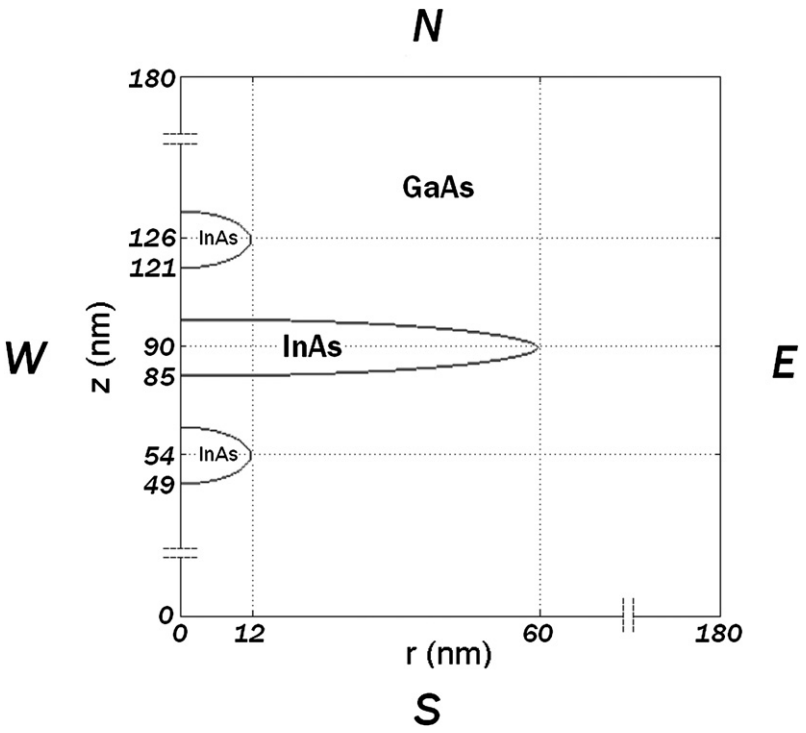

Fig. 1. Three vertically aligned InAs/GaAs quantum dots with cylindrically symmetric domain in real space dimensions in nano meters that are used in numerical implementation. The domain in 2D setting is denoted by Ω with the boundary $\partial\Omega$ consisting of the south (S), east (E), north (N), and west (W) sides.

realistic finite confinement potential with band nonparabolicity that leads to an energy-dependent mass in the Hamiltonian for electrons. The nonparabolicity is derived from a projection from the eight-band Kane Hamiltonian into the 2×2 conduction space and hence gives more accurate results as shown in [20–23].

The CSDFT applied to the QDM system with three-dimensionality of the finite confinement and band nonparabolicity poses a very challenging task for the numerical implementation. The energy-dependent mass in the Hamiltonian results in a cubic eigenvalue problem from, e.g., a finite difference discretization. The Jacobi–Davidson (JD) method developed in [24,25] is extended and incorporated into a self-consistent algorithm for solving the Schrödinger–Poisson system that implements the CSDFT in real space. We also give a detailed description of the computational algorithm, the Poisson solver, and the approximation methods for the xc energy.

Numerical results on the Kohn–Sham (KS) orbitals and energies of six electrons in the molecule with some magnetic fields are presented in detail. It is shown that the six electrons residing in the central dot at zero magnetic field can be changed to such that each dot contains two electrons with some feasible magnetic field. The Förster energy transfer may therefore be generated by two individual QDMs. This may motivate a new paradigm of Fermionic qubits for quantum computing in solid-state systems, which will be reported in a coming paper.

2. The current spin density functional theory for the model system

The density functional theory (DFT) introduced in the two seminal papers [26,27] is perhaps the most successful approach to compute the electronic structure of matter ranging from atoms, molecules, to solids. Vignale and Rasolt developed an extension of DFT that makes it possible to include gauge fields in the energy functional [15,16] and has been widely used to describe the electronic structure of quantum dots in magnetic fields [17–19,28].

In CSDFT, the ground state energy of an interacting system with electron number N and the total spin S in the local external potential $V_{\text{ext}}(\mathbf{r})$ is a functional of spin density $n^\sigma(\mathbf{r})$, with $\sigma = \uparrow, \downarrow$ (or ± 1) denoting spin-up and spin-down, respectively,

$$E(n) = T(n) + \int n(\mathbf{r})\left[V_{\text{ext}}(\mathbf{r}) + \frac{1}{2}V_H(\mathbf{r})\right]\mathrm{d}\mathbf{r} + E_B(n) + E_{\text{xc}}(n), \tag{2.1}$$

where the total density $n(\mathbf{r}) = n^\uparrow(\mathbf{r}) + n^\downarrow(\mathbf{r})$ and the spin densities satisfy the constraint $\int n^\sigma(\mathbf{r})\,\mathrm{d}\mathbf{r} = N^\sigma$ with $N^\uparrow = (N + 2S)/2$, and $N^\downarrow = (N - 2S)/2$ [28]. Assuming that the ground state of the noninteracting reference system is nondegenerate, the noninteracting kinetic energy is expressed as

$$T(n) = \sum_{j,\sigma}\langle\Psi_{j\sigma}|\Pi\left(\frac{1}{2m(\mathbf{r},\varepsilon_{j\sigma})}\right)\Pi|\Psi_{j\sigma}\rangle, \tag{2.2}$$

where $\Pi = -i\hbar\nabla + e\mathbf{A}(\mathbf{r})$ denotes the electron momentum operator, $\hbar$ is the reduced Planck constant, e is the proton charge, $\mathbf{A}(\mathbf{r}) = \frac{B}{2}(-y, x, 0)$ is the vector potential induced by an external magnetic field $\mathbf{B} = \operatorname{curl}\mathbf{A} = B\hat{z}$ applied perpendicular to the xy plane, and $\Psi_{j\sigma}$ and $\varepsilon_{j\sigma}$ are Kohn–Sham (KS) orbitals and eigenvalues to be specified below. The effect of band nonparabolicity leads to the mass depending on both energy and

Table 1
Numerical values of all parameters used in this paper

	Value	Unit	Formula	Reference
e	1.60219×10^{-19}	C		
B		T		
$\hbar$	1.05459×10^{-34}	Js		
p(InAs)	1.20311×10^{-28}		$3m_0p^2/\hbar^2$	[29]
p(GaAs)	1.25614×10^{-28}			
m_0	9.10956×10^{-31}	kg		
E_g(InAs)	0.421	eV		[29]
E_g(GaAs)	1.52	eV		[29]
$\mathbf{\Delta}$(InAs)	0.48	eV		[29]
$\mathbf{\Delta}$(GaAs)	0.34	eV		[29]
V_0	0.77	eV		[29]
ϵ_0	8.854187×10^{-12}	F/m		
ϵ_{InAs}	12.2			[20]
ϵ_{GaAs}	12.7			
μ_B	9.2741×10^{-24}	J/T		
c	2.997925×10^{8}	m/s		

position, which is defined by [20]

$$\frac{1}{m(\mathbf{r},\varepsilon_{j\sigma})} = \frac{p^2}{\hbar^2}\left[\frac{2}{\varepsilon_{j\sigma} + E_g(\mathbf{r}) - V_{\text{ext}}(\mathbf{r})} + \frac{1}{\varepsilon_{j\sigma} + E_g(\mathbf{r}) - V_{\text{ext}}(\mathbf{r}) + \Delta(\mathbf{r})}\right], \tag{2.3}$$

where $E_g(\mathbf{r})$ and $\mathbf{\Delta}(\mathbf{r})$ are energy-band gap and spin-orbit splitting in the valence band, respectively, and p is the momentum matrix element. These parameters are material (position) dependent. We denote the spatial domain of the model, i.e. Fig. 1, as $\overline{\Omega} = \overline{\Omega}_{\text{InAs}} \cup \overline{\Omega}_{\text{GaAs}} \subset R^3$, where the three InAs quantum dots are embedded in the GaAs matrix. All numerical values of the parameters used in this paper are listed in Table 1, which also includes the corresponding units and cited references.

The hard-wall confinement potential V_{ext} is induced by a discontinuity of conduction-band edge of the system components and is given as

$$V_{\text{ext}}(\mathbf{r}) = \begin{cases} 0, & \text{in } \overline{\Omega}_{\text{InAs}}, \\ V_0, & \text{in } \overline{\Omega}_{\text{GaAs}}. \end{cases} \tag{2.4}$$

The Hartree potential is defined as

$$V_H(\mathbf{r}) = \frac{e^2}{4\pi\epsilon_0\epsilon(\mathbf{r})}\int \frac{n(\mathbf{r}')}{|\mathbf{r}-\mathbf{r}'|}\,d\mathbf{r}', \tag{2.5}$$

where ϵ_0 the permittivity of vacuum and $\epsilon(\mathbf{r})$ is the dielectric constant of the background material.

The vector field $\mathbf{A}(\mathbf{r})$ adds extra terms to the energy functional as follows

$$E_B(n) = \frac{1}{2}g\mu_B B\int\left[n^{\uparrow}(\mathbf{r}) - n^{\downarrow}(\mathbf{r})\right]d\mathbf{r} + e\int \mathbf{j}_p(\mathbf{r})\cdot\mathbf{A}(\mathbf{r})\,d\mathbf{r}, \tag{2.6}$$

where g is the Landé factor, μ_B is the Bohr magneton, and

$$\mathbf{j}_p(\mathbf{r}) = \frac{-i\hbar}{2m}\sum_{i,\sigma}\left[\Psi^*_{j\sigma}(\mathbf{r})\nabla\Psi_{j\sigma}(\mathbf{r}) - \Psi_{j\sigma}(\mathbf{r})\nabla\Psi^*_{j\sigma}(\mathbf{r})\right]$$

is the paramagnetic current density.

The xc energy $E_{\text{xc}}(n)$ is defined as

$$E_{\text{xc}}(n) = E_x(n) + E_c(n) = \int n(\mathbf{r})\varepsilon_{\text{xc}}(n,\gamma)\,d\mathbf{r}, \tag{2.7}$$

where the xc energy per particle ε_{xc} depends on the field B internal structure of the wave function. It formally depends on the vorticity

$$\gamma(\mathbf{r}) = \nabla\times\frac{\mathbf{j}_p(\mathbf{r})}{n(\mathbf{r})}\bigg|_z. \tag{2.8}$$

To minimize the total energy of the system, a functional derivative of $E(n)$ is taken with respect to $\Psi^*_{j\sigma}$ under the constraint of the orbitals $\Psi_{j\sigma}$ being normalized. The resulting KS equations are

$$\mathbf{H}^{\sigma}_{\text{KS}}\Psi_{j\sigma} = \varepsilon_{j\sigma}\Psi_{j\sigma} \tag{2.9}$$

with the KS Hamiltonian $\mathbf{H}^{\sigma}_{\text{KS}}$ defined as

$$\mathbf{H}^{\sigma}_{\text{KS}} = -\Pi\left(\frac{1}{2m(\mathbf{r},\varepsilon_{j\sigma})}\right)\Pi + V_{\text{ext}}(\mathbf{r}) + V_B(\mathbf{r}) + V_H(\mathbf{r}) + V^{\sigma}_{\text{xc}}(\mathbf{r}), \tag{2.10}$$

where

$$V_B(\mathbf{r}) = \sigma\frac{1}{2}g(\mathbf{r},\varepsilon_{j\sigma})\mu_B B, \tag{2.11}$$

$$g(\mathbf{r},\varepsilon_{j\sigma}) = 2\left\{1 - \frac{m_0}{m(\mathbf{r},\varepsilon_{j\sigma})}\frac{\mathbf{\Delta}(\mathbf{r})}{3(\varepsilon_{j\sigma} + E_g(\mathbf{r}) - V_{\text{ext}}(\mathbf{r}) + 2\mathbf{\Delta}(\mathbf{r})}\right\}, \tag{2.12}$$

and $\sigma = \pm 1$ referring to the orientation of the electron spin along the z-axis. The xc potential

$$V^{\sigma}_{\text{xc}}(\mathbf{r}) = \frac{\delta[n(\mathbf{r})\varepsilon_{\text{xc}}(n,\gamma)]}{\delta n^{\sigma}} - \frac{e}{n}\mathbf{j}_p\cdot\mathbf{A}_{\text{xc}}, \tag{2.13}$$

where $\mathbf{A}_{\text{xc}}$ is the xc vector potential defined by

$$e\mathbf{A}_{\text{xc}} = \frac{1}{n}\left(\frac{\partial}{\partial y}\frac{\delta[n(\mathbf{r})\varepsilon_{\text{xc}}(n,\gamma)]}{\delta\gamma}, -\frac{\partial}{\partial x}\frac{\delta[n(\mathbf{r})\varepsilon_{\text{xc}}(n,\gamma)]}{\delta\gamma}, 0\right). \tag{2.14}$$

We use the LSDA for calculating the xc energy. In CSDFT, the LSDA has to be extended to include the orbital currents. Following Vignale and Rasolt [16], the xc vector potential is approximated as

$$\frac{e}{c}\mathbf{A}_{\text{xc},\sigma} \approx \frac{-\bar{b}}{n_{\sigma}(\mathbf{r})}\nabla\times\left[\nabla\times\frac{\mathbf{j}_{p\sigma}(\mathbf{r})}{n_{\sigma}(\mathbf{r})}\right], \tag{2.15}$$

where

$$-\bar{b} = \frac{mk_F}{48\pi^2}\left[\frac{\chi_L}{\chi^0_L} - 1\right] \tag{2.16}$$

with k_F being the Fermi momentum and $\frac{\chi_L}{\chi^0_L}$ the diamagnetic-susceptibility ratio. The values of this ratio are tabulated in [30].

For the xc energy functional ε_{xc} in (2.13), we adopt the form developed by Perdew and Wang [31] as

$$\varepsilon^{\text{PW}}_{\text{xc}}(n,\zeta) = \varepsilon_x(r_s,\zeta) + \varepsilon_c(r_s,\zeta), \tag{2.17}$$

where

$$\varepsilon_x(r_s,\zeta) = -\frac{3}{4\pi r_s}\left[\frac{9\pi}{4}\right]^{1/3}\frac{[(1+\zeta)^{4/3}+(1-\zeta)^{4/3}]}{2}, \quad (2.18)$$

$$\varepsilon_c(r_s,\zeta) = \varepsilon_c(r_s,0) + \alpha_c(r_s)\frac{f(\zeta)}{f''(0)}(1-\zeta^4) + \big[\varepsilon_c(r_s,1) - \varepsilon_c(r_s,0)\big]f(\zeta)\zeta^4, \quad (2.19)$$

$\zeta = (n^{\uparrow}(\mathbf{r}) - n^{\downarrow}(\mathbf{r}))/n(\mathbf{r})$ is the spin polarization, $r_s = (\frac{3}{4\pi n})^{1/3}$ is the Wigner–Seitz radius, and the functions $\varepsilon_c(r_s,0)$, $\varepsilon_c(r_s,1)$, and $-\alpha_c(r_s)$ are given in [31]. Note that the magnetic field dependence on the correlation energy, which might affect the total energies and spin configurations, is not taken into account in the present formula.

3. Numerical methods and algorithms for the model system

Since the three QDs and the magnetic field are cylindrically symmetric, the wave function, the spin density, and the paramagnetic current density can be represented as

$$\Psi_q(\mathbf{r}) = e^{-il\theta}\phi_q(r,z), \quad q \equiv \{nl\sigma\} \quad (3.1)$$

$$n^{\sigma}(\mathbf{r}) = n^{\sigma}(r,z) = \sum_{q}^{N^{\sigma}}\big|\phi_q(r,z)\big|^2, \quad (3.2)$$

$$\mathbf{j}_p(\mathbf{r}) = -\frac{\hbar}{m(r,z,\varepsilon_q)}\sum_{q}^{N} l\big|\phi_q(r,z)\big|^2\hat{\mathbf{e}}_{\theta}, \quad (3.3)$$

where n is the principal quantum number, $l = 0, \pm1, \pm2, \ldots$, is the quantum number of the projection of angular momentum onto the magnetic field axis, i.e. the z-axis and $\hat{\mathbf{e}}_{\theta}$ is the azimuthal unit vector. The KS equations are then reduced to a 2D problem in the (r,z) coordinates as

$$\mathbf{H}_{\mathrm{KS}}^{l\sigma}\phi_q(r,z) = \varepsilon_q\phi_q(r,z), \quad (3.4)$$

where the KS Hamiltonian is now defined by

$$\mathbf{H}_{\mathrm{KS}}^{l\sigma} = T_S + T_B + V_{\mathrm{ext}} + V_B + V_H + V_{\mathrm{xc}}, \quad (3.5)$$

$$T_S(r,z) = -\frac{\hbar^2}{2m(r,z,\varepsilon_q)}\left(\frac{\partial^2}{\partial r^2} + \frac{1}{r}\frac{\partial}{\partial r} - \frac{l^2}{r^2} + \frac{\partial^2}{\partial z^2}\right), \quad (3.6)$$

$$T_B(r,z) = \frac{e^2B^2r^2}{8m(r,z,\varepsilon_q)} + \frac{\hbar eBl}{2m(r,z,\varepsilon_q)}. \quad (3.7)$$

In 2D setting, the solution domain for (3.4) is again expressed by the same notation as that of 3D, that is, $\overline{\Omega} = \overline{\Omega}_{\mathrm{InAs}} \cap \overline{\Omega}_{\mathrm{GaAs}} \subset R^2$. We choose the domain $\overline{\Omega}_{\mathrm{GaAs}}$ sufficiently large so that the wave function is negligibly small at the boundary of $\overline{\Omega}_{\mathrm{GaAs}}$. By symmetry, the domain $\overline{\Omega}$ can be reduced to $\overline{\Omega} = \{(r,z)\colon\ 0 \leqslant r \leqslant r_{\max}, -z_{\max} \leqslant z \leqslant z_{\max}\}$ for sufficiently large $r_{\max} > 0$ and $z_{\max} > 0$ as shown in Fig. 1.

The explicit formula for the potential $V_{\mathrm{xc}}(\mathbf{r})$ in (2.13) is extremely complex in 3D coordinates. Transforming it to the (r,z) space is prohibitively lengthy and impractical. We use all the original formulas (2.13)–(2.19) for calculating $V_{\mathrm{xc}}(\mathbf{r})$ in the 3D space and then obtain the potential in the (r,z) coordinates, i.e. $V_{\mathrm{xc}}(r,z)$ for (3.4).

Since we are dealing with the hard-wall confinement potential, the interface conditions of the wave function in (3.4) has to be specifically imposed, namely,

$$\begin{cases} \frac{1}{2m(r,z,\varepsilon_q)}\Pi\phi_q(r,z)\cdot\mathbf{n}|_{\Gamma^-} = \frac{1}{2m(r,z,\varepsilon_q)}\Pi\phi_q(r,z)\cdot\mathbf{n}|_{\Gamma^+}, \\ \phi_q(r,z)|_{\Gamma^-} = \phi_q(r,z)|_{\Gamma^+}, \end{cases} \quad (3.8)$$

where Γ denotes the interface between two materials, i.e. $\Gamma = \overline{\Omega}_{\mathrm{InAs}} \cap \overline{\Omega}_{\mathrm{GaAs}}$, $\mathbf{n}$ is an outward normal unit vector on the boundary of Ω_{InAs}, and Γ^- and Γ^+ are the sets of limiting points to the curve Γ from the interior and the exterior of Ω_{InAs}, respectively. The momentum operator Π is similarly defined for the 2D case. The boundary conditions for (3.4) are

$$\begin{cases} \phi_q(r,z)|_{W^-} = \phi_q(r,z)|_{W^+}, \\ \phi_q(r,z) = 0, \quad \text{on } S,\ E,\ N, \end{cases} \quad (3.9)$$

where W, S, E, and N denotes the west, south, east, and north side boundaries of the domain $\overline{\Omega}$. Note that on the west side of the boundary the values of the wave function are taken to be the same for satisfying the continuity condition across W. In actual implementation this condition is replaced by taking the values of the two horizontal grid points adjacent to W as the same. Moreover, to avoid numerical over-flow due to the term $1/r$ in (3.6), we do not define unknowns at the grid points on W.

Note that the potential functions $V_{\mathrm{ext}}(\mathbf{r})$ and $V_B(\mathbf{r})$ can be directly reduced to the (r,z) space since these functions are independent of the azimuthal coordinate. In real space approximation, the Hartree potential $V_H(\mathbf{r})$ is usually calculated by solving the Poisson equation [32]

$$\nabla\cdot\epsilon(\mathbf{r})\nabla V_H(\mathbf{r}) = -\frac{e^2}{4\pi\epsilon_0}n(\mathbf{r}). \quad (3.10)$$

By cylindrical symmetry, this equation can be written as

$$\left(\frac{\partial^2}{\partial r^2} + \frac{1}{r}\frac{\partial}{\partial r} + \frac{1}{r^2}\frac{\partial^2}{\partial\theta^2} + \frac{\partial^2}{\partial z^2}\right)V_H(r,\theta,z) = f(r,z), \quad (3.11)$$

$$f(r,z) = -\frac{e^2}{4\pi\epsilon_0\epsilon_i}\sum_{q}^{N}\big|\phi_q(r,z)\big|^2, \quad \text{for } i = 1 \text{ or } 2, \quad (3.12)$$

where $\epsilon_1 = \epsilon_{\mathrm{InAs}}$ if $(r,z) \in \overline{\Omega}_{\mathrm{InAs}}$ and $\epsilon_2 = \epsilon_{\mathrm{GaAs}}$ if $(r,z) \in \overline{\Omega}_{\mathrm{GaAs}}$. By using the method of separating variables and substituting a solution of the form

$$V_H(r,\theta,z) = V_H(r,z)V(\theta) \quad (3.13)$$

into (3.11), we have

$$V(\theta)\left(\frac{\partial^2}{\partial r^2} + \frac{1}{r}\frac{\partial}{\partial r} + \frac{\partial^2}{\partial z^2}\right)V_H(r,z) + V_H(r,z)\frac{1}{r^2}\frac{\partial^2V(\theta)}{\partial\theta^2} = f(r,z)$$

or

$$\frac{V(\theta)r^2}{V_H(r,z)}\left(\frac{\partial^2}{\partial r^2} + \frac{1}{r}\frac{\partial}{\partial r} + \frac{\partial^2}{\partial z^2}\right)V_H(r,z) + \frac{\partial^2V(\theta)}{\partial\theta^2} = \frac{r^2}{V_H(r,z)}f(r,z). \quad (3.14)$$

Obviously, by setting $V(\theta) = k$ where k is an arbitrary constant, a function $V_H^p(r,z) = kV_H(r,z)$ satisfying the 2D Poisson equation

$$\left(\frac{\partial^2}{\partial r^2} + \frac{1}{r}\frac{\partial}{\partial r} + \frac{\partial^2}{\partial z^2}\right) V_H^p(r,z) = f(r,z) \tag{3.15}$$

is a particular solution of (3.14) in view of a second order nonhomogeneous ordinary differential equation with respect to θ. The corresponding homogeneous general solution is $e^{ik\theta}V_H^h(r,z)$ satisfying the Laplace equation

$$\left(\frac{\partial^2}{\partial r^2} + \frac{1}{r}\frac{\partial}{\partial r} + \frac{\partial^2}{\partial z^2} - \frac{k^2}{r^2}\right) V_H^h(r,z) = 0. \tag{3.16}$$

The general solution of the nonhomogeneous equation (3.14) is therefore of the form

$$\sum_k e^{ik\theta} V_H^h(r,z) + V_H^p(r,z). \tag{3.17}$$

In 2D setting, we also have similar interface conditions for Poisson's problem (3.10), namely,

$$\begin{cases} \epsilon(r,z)\nabla V_H^p(r,z)\cdot\mathbf{n}|_{\Gamma^-} = \epsilon(r,z)\nabla V_H^p(r,z)\cdot\mathbf{n}|_{\Gamma^+}, \\ V_H(r,z)|_{\Gamma^-} = V_H(r,z)|_{\Gamma^+}. \end{cases} \tag{3.18}$$

Similarly, the boundary conditions for (3.10) are

$$\begin{cases} V_H^p(r,z)|_{W^-} = V_H^p(r,z)|_{W^+}, \\ V_H^p(r,z) = 0, \quad \text{on } S,\ E,\ N. \end{cases} \tag{3.19}$$

By imposing these boundary conditions to the general solution (3.17), we deduce that the particular solution $V_H^p(r,z)$ is in fact a general solution of (3.14) and thus of (3.11), i.e. $V_H^h(r,z) = 0$.

Note that for atomic systems the far side boundary condition of the Hartree potential is usually taken the values obtained by using efficient multipole expansion techniques [33]. For our model problem, the size of the domain is $180 \times 180\ \text{nm}^2$ which in comparison with that of atomic systems is quite large and hence the zero boundary condition for the potential on the far side of the boundary is numerically feasible, see Section 4 below for numerical evidence on the choice of the size.

We then use the standard finite difference method to approximate our model problem. Since the mass in (2.3) and the Landé factor of (2.12) are energy dependent, the KS equation (3.4) and its interface and boundary conditions (3.8) and (3.9) will result in a system of cubic eigenvalue equations

$$\left(A_0 + \lambda A_1 + \lambda^2 A_2 + \lambda^3 A_3\right)\mathbf{x} = 0, \tag{3.20}$$

where the unknown eigenpair $(\lambda, \mathbf{x})$ is an approximate solution of (ε_q, ϕ_q) for some q. Starting from the Schrödinger equation, finite difference discretization, to the coefficient matrices A_0, A_1, A_2, and A_3, a detailed derivation of a similar cubic eigenvalue system is given in [24] for a single-particle quantum dot model. Several Jacobi–Davidson methods are proposed and compared in [25] for solving this type of eigenvalue problems.

Analogously, the Poisson equation (3.15) with its interface and boundary conditions (3.18) and (3.19) leads to a system of algebraic equations

$$A\mathbf{x} = \mathbf{b}, \tag{3.21}$$

where now the unknown vector $\mathbf{x}$ corresponds to the approximate values of $V_H(r,z)$ at the grid points.

We briefly describe our algorithm for the implementation of the model system in CSDFT as follows:

Algorithm 1. A self-consistent method for the current spin density functional theory.

(1) Set $V_H = 0$, $V_{\text{xc}} = 0$, and solve (3.20) for $\phi_q^{(0)}(r,z)$ with $\sigma = \uparrow$ and then with $\sigma = \downarrow$ by using the cubic Jacobi–Davidson method. Set $k = 0$. When $B = 0$, the first three lowest energies correspond to $n = 1$ and $l = 0, 1, 2$. We therefore must solve (3.20) six times. At each time, we only seek for the smallest eigenpair. As for $B = 15$, the first three lowest energies correspond to $n = 1, 2, 3$ and $l = 0$. We thus solve (3.20) two times. At each time, we then seek for the three smallest eigenpairs.
(2) Evaluate the electron densities $n^{\uparrow}(\mathbf{r})$, $n^{\downarrow}(\mathbf{r})$, $n(\mathbf{r})$, and the electron energies $E_q^{(k)}$. If the energies converge within an error tolerance then stop. Otherwise, set $k = k + 1$.
(3) Solve (3.21) for the Hartree potential V_H by using GMRES [34].
(4) Evaluate V_{xc} via (2.13) and then solve (3.20) for the next iterate $\phi_q^{(k)}(r,z)$. Go to (2).

There are several numerical issues deserved to be elaborated due to the special formulation of the present model when compared with the existing models of multielectronic systems of QDs. The most prominent feature of the present model is the nonparabolic dispersion relation used to define the effective mass (2.3), the Landé factor (2.12), and the interface condition (3.8). As a result, the set of eigenvalues that interests us is embedded in the interior of the spectrum of the eigenvalue problem (3.20) which is a nonsymmetric system. Moreover, with some feasible magnetic fields, we expect to have degenerate eigenstates due to the two identical smaller dots, i.e. the eigenvalue system is defective. In stead of using deflation scheme in the JD solver [25], we extend the generalized Davidson method of Crouzeix, Philippe, and Sadkane [35] to our cubic JD method that allows us to compute several eigenpairs simultaneously and to have a block implementation of Krylov subspaces and search direction transformation. Our JD algorithm is summarized as follows:

Algorithm 2. A cubic Jacobi–Davidson method.

(1) Choose an arbitrary orthonormal matrix $V := [v_1, \ldots, v_n]$ and let K be a given integer that limits the dimension of the basis of the subspace. Here n can be taken as 3 for six electrons with spin-up and spin-down.
(2) Compute $W_k = A_k V$ and $M_k = V^* W_k$, for $k = 0, 1, 2, 3$, where the matrices A_k are given in (3.20).
(3) For $j = n, \ldots, K$, do
  (3a) Compute the eigenpairs of $(\theta^3 M_3 + \theta^2 M_2 + \theta M_1 + M_0)\phi = 0$ by solving the generalized linear eigen-

value problem

$$\begin{bmatrix} 0 & I & 0 \\ 0 & 0 & I \\ M_0 & M_1 & M_2 \end{bmatrix} \begin{bmatrix} s \\ \theta s \\ \theta^2 s \end{bmatrix} = \theta \begin{bmatrix} I & & \\ & I & \\ & & -M_3 \end{bmatrix} \begin{bmatrix} s \\ \theta s \\ \theta^2 s \end{bmatrix}$$

using the QZ algorithm [36].

(3b) Select the desired eigenpairs (θ_i, ϕ_i) with $\|\phi_i\|_2 = 1$, for $i = 1, \ldots, n$.

(3c) For $i = 1, \ldots, n$, compute the Ritz vectors $u_i = V\phi_i$, the residuals $r_i = A(\theta_i)u_i$, and $p_i = A'(\theta_i)u_i$, where $A(\theta_i) := A_0 + \theta_i A_1 + \theta_i^2 A_2 + \theta_i^3 A_3$ and $A'(\theta_i) := A_1 + 2\theta_i A_2 + 3\theta_i^2 A_3$.

(3d) If $\|r_i\|_2 < \text{Tol}$, for $i = 1, \ldots, n$, then stop.

(3e) If $K - j < n$, then go to step (4).

(3f) For $i = 1, \ldots, n$, do

- If $\|r_i\|_2 < \text{Tol}$, then go to step (3f).
- Compute the correction $t = -M_A^{-1} r_i + \varepsilon M_A^{-1}$, where $\varepsilon = \frac{u_i^* M_A^{-1} r_i}{u_i^* M_A^{-1} p_i}$ and M_A is a preconditioner (by SSOR) of $A(\theta_i)$.
- Orthonormalize t against V by the modified Gram–Schmidt (MGS) method.
- For $k = 0, 1, 2, 3$, compute $w_k = A_k t$, $M_k = \begin{bmatrix} M_k & V^* w_k \\ t^* W_k & v^* w_k \end{bmatrix}$.
- Expand $V = [V, t]$ and $W_k = [W_k, w_k]$, for $k = 0, 1, 2, 3$.
- Set $j = j + 1$.

(4) Use n Ritz vectors $u_1, \ldots, u_n$ to create a new $V := MGS(u_1, \ldots, u_n)$ and go to step (2) for restarting.

Note that the classical approach for dealing with the nonlinear matrix equation (3.20) is to transform the equation into a generalized linear eigenvalue system with the matrix dimension of 3 times that of (3.20) and then solve the system by the Lanczos or Arnoldi method. The matrix dimension of (3.20) for the present QDM model is about 290 000. The JD method described here instead solves the generalized linear eigenvalue system in step (3a) in a much smaller subspace V. The matrix dimension of the matrices M_i, $i = 0, 1, 2, 3$, is about 50 in our numerical implementation. The matrix dimension of the linearized system in step (3a) is thus about 150. The KS Hamiltonian (2.10) is based on the nonparabolic band structure approximation. If the Hamiltonian is based on the Kane's original form, the resulting eigenvalue problem will then be of linear form but with the matrix dimension of 4 times that of (3.20). The nonparabolic approximation thus reduces computational efforts significantly at the cost of more delicate nonlinear eigenvalue systems.

4. Numerical results

For the proposed model, we first determine the size of the domain in Fig. 1 by inspecting the rate of change of the first three energy levels with respect to $r_{\max} = z_{\max}$. As shown in Fig. 2, the change of these energies around $r_{\max} = 180$ nm and beyond is relatively small. The following numerical results are thus based on the domain with $r_{\max} = 180$ nm.

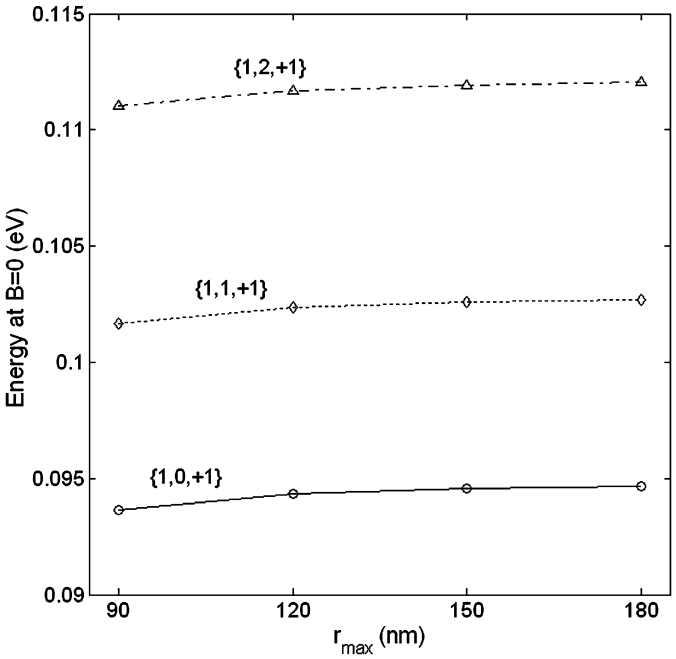

Fig. 2. The effect of the domain size on the first three energies at $B = 0$.

Table 2
Energies for the nonparabolic and parabolic approximation at $B = 0$ in units of eV

$q = \{nl\sigma\}$	Nonparabolic	Parabolic
$\{1, 0, +1\}$	0.094673	0.086873
$\{1, 1, +1\}$	0.102689	0.095749
$\{1, 2, +1\}$	0.112039	0.106298

We next present the important effect of the band nonparabolicity. In Table 2, we observe that the energy differences between the parabolic and nonparabolic dispersion relations used in the Hamiltonian for zero magnetic field can be very significant since the magnitudes are comparable with that of the exchange energies as shown in Table 3. For the parabolic dispersion case, the effective mass in (2.2) is taken as $m = 0.024 m_0$. In Tables 3 and 4, all energy components in (3.5) are separately presented to indicate the magnitudes of the energies from various effects. Here, the total ground-state energy E obtained via the KS eigenvalues ε_q is defined by [16]

$$E = \sum_q^N E_q = \sum_q^N \varepsilon_q - \frac{1}{2} \frac{e^2}{4\pi\epsilon_0 \epsilon(\mathbf{r})} \iint \frac{n(\mathbf{r}) n(\mathbf{r}')}{|\mathbf{r} - \mathbf{r}'|} \, d\mathbf{r}' \, d\mathbf{r} - \sum_\sigma \int V_{\text{xc}}^\sigma(\mathbf{r}) n^\sigma(\mathbf{r}) \, d\mathbf{r} - \frac{e}{c} \int \mathbf{j}_p \cdot \mathbf{A}_{\text{xc}} \, d\mathbf{r} + E_{\text{xc}}(n).$$

As stated above, our main concern for the present QDM model is to show the state change of the electrons under the influence of magnetic fields. The wave functions of the six electrons originally occupying the lowest 3 energy states with $B = 0$ as given in Table 3 are shown in the left panel of Fig. 3,

Table 3
Energies at $B = 0$ in units of eV

q	$\{1, 0, +1\}$	$\{1, 1, +1\}$	$\{1, 2, +1\}$
E_q	0.094673	0.102689	0.112039
$\langle T_S \rangle$	0.067484	0.075638	0.084511
$\langle T_B \rangle$	0	0	0
$\langle V_{\text{ext}} \rangle$	0.019227	0.020536	0.022024
E_B	0	0	0
$\frac{1}{2}\langle V_H \rangle$	0.015120	0.013653	0.012280
E_x	−0.006772	−0.006753	−0.006398
E_c	−0.000386	−0.000385	−0.000378

Table 4
Energies at $B = 15$ in units of eV E_q^* are energies based on the single-particle Hamiltonian

q	$\{1, 0, +1\}$	$\{2, 0, +1\}$	$\{3, 0, +1\}$	$\{1, 0, -1\}$	$\{2, 0, -1\}$	$\{3, 0, -1\}$
E_q^*	0.103250	0.134668	0.134668	0.114840	0.146072	0.146072
E_q	0.113092	0.146387	0.147649	0.120784	0.153012	0.154220
$\langle T_S \rangle$	0.078144	0.114168	0.113827	0.077302	0.113209	0.112880
$\langle T_B \rangle$	0.008975	0.002510	0.002499	0.008889	0.002484	0.002473
$\langle V_{\text{ext}} \rangle$	0.017801	0.021184	0.021067	0.017713	0.021108	0.020994
E_B	−0.004436	−0.003913	−0.003877	0.004325	0.003832	0.003798
$\frac{1}{2}\langle V_H \rangle$	0.021932	0.026358	0.028058	0.021925	0.026359	0.028059
E_x	−0.008884	−0.013414	−0.013418	−0.008877	−0.013419	−0.013422
E_c	−0.000441	−0.000506	−0.000506	−0.000493	−0.000562	−0.000562

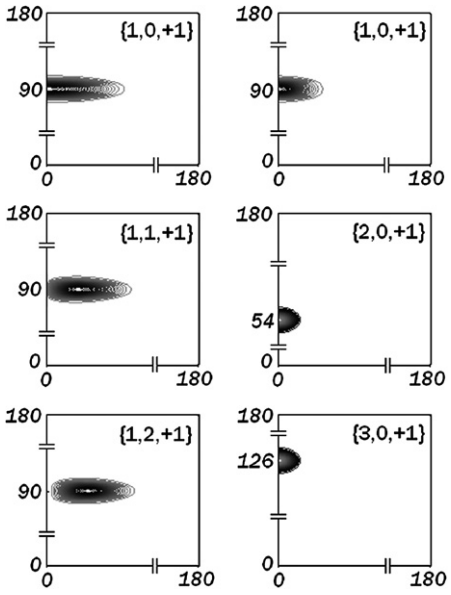

Fig. 3. Contour of KS orbitals at $B = 0$ (left panel) and $B = 15$ (right panel).

which clearly illustrates that the electrons are residing in the central dot. For $B = 15$, we see that, corresponding to the lowest 6 energy states as given in Table 4, each one of these three dots contains two electrons for which their wave functions are shown in the right panel of Fig. 3. Note that three-dimensional wave functions can be easily illustrated from these two-dimensional wave functions via the formula (3.1).

Accuracy of the exchange energies can be verified by the ratio between the absolute values of $\frac{1}{2}\langle V_H \rangle$ and E_x, which is about 2 for two-electron atoms [37]. It has been theoretically shown in [38] that this ratio is exactly equal to 2 for a two-electron model for which the xc energy and xc potential can be determined exactly in an external harmonic potential. From Tables 3 and 4, the ratio is approximately 2.

Finally, we remark that the essential physics of this study, namely the state change of electrons in QDM under the influence of magnetic field as such indicated by Fig. 3, can also be simulated by means of a much simpler model, e.g., the single-particle Hamiltonian with parabolic band structure (i.e., constant effective mass approximation). However, the numerics of the computed energies can be quite different from that of the present model as shown by the numbers in the second and third rows in Table 4. Moreover, we may obtain degenerate states such as $\{2, 0, +1\}$ and $\{3, 0, +1\}$ under the single-particle picture, which obviously is incorrect. In addition to the effect of the model in use, the state change is significantly governed by the QDM dimensions as given in Fig. 1 so that we can attain the electronic behavior as shown in Fig. 3. These dimensions are also experimentally feasible [9].

5. Conclusion

A new mathematical model that incorporates the nonparabolic energy dispersion relation and realistic hard-wall finite confinement potential into the many-body Hamiltonian in the current spin density functional theory in 3D setting is proposed. It is used to study the electronic properties of a quantum dot molecule that consists of three vertically aligned semiconductor quantum dots (one large central dot and two smaller identical dots) under the influence of magnetic fields. A new Jacobi–Davidson method is given to solve the cubic eigenvalue problem resulting from finite difference approximation due to the nonparabolic nature of the effective mass. It is shown that the effect of band nonparabolicity can be very significant in the sense that the energy difference between the parabolic and nonparabolic cases is comparable with that of exchange energies in multielectronic system. Furthermore, we show that six electrons residing in the large central dot at zero magnetic field can be changed to such that each dot contains two electrons with some feasible magnetic field.

This paper is intended to describe mathematical aspects of the model and to present preliminary physical results only on the Kohn–Sham orbitals and detailed energy components with two different magnetic fields. Following this more realistic and accurate model, there are many interesting physical phenomena such as capacitance, optical and transport properties, Wigner crystallization, Aharonov–Bohm oscillation, and quantum Hall effect can be further investigated for semiconductor nanostructures in three dimensional space. In particular, with an additional electric control, we expect to have an energy selective mechanism to manipulating excitonic states of two closely spaced QDMs so that a strong coherent dipole–dipole coupling can be achieved and hence the Förster–Dexter resonant energy transfer between QDMs can be realized to motivate a new paradigm of Fermionic qubits for quantum computing in solid-state systems.

Acknowledgements

The authors would like to thank J.-Y. Hsu, T.-F. Jiang, and C. Wu of the first principle group at NCTU for valuable discussions on DFT. The authors are grateful for referees' comments.

References

[1] D.P. DiVincenzo, Science 270 (1995) 255.
[2] B.E. Kane, Nature 393 (1998) 133.
[3] A. Imamoglu, D.D. Awschalom, G. Burkard, D.P. DiVincenzo, D. Loss, M. Sherwin, A. Small, Phys. Rev. Lett. 83 (1999) 4204.
[4] E. Biolatti, R.C. Iotti, P. Zanardi, F. Rossi, Phys. Rev. Lett. 85 (2000) 5647.
[5] P.M. Petroff, A. Lorke, A. Imamoglu, Phys. Today 54 (2001) 46.
[6] M. Bayer, P. Hawrylak, K. Hinzer, S. Fafard, M. Korkusinski, Z.R. Wasilewski, O. Stern, A. Forchel, Science 291 (2001) 451.
[7] B.W. Lovett, J.H. Reina, A. Nazir, G.A.D. Briggs, Phys. Rev. B 68 (2003) 205319.
[8] J.M. Elzerman, R. Hanson, L.H. Willems van Beveren, B. Witkamp, L.M.K. Vandersypen, L.P. Kouwenhoven, Nature 430 (2004) 431.
[9] G. Ortner, I. Yugova, G. Baldassarri Höger von Högersthal, A. Larionov, H. Kurtze, D.R. Yakovlev, M. Bayer, S. Fafard, Z. Wasilewski, P. Hawrylak, Y.B. Lyanda-Geller, T.L. Reinecke, A. Babinski, M. Potemski, V.B. Timofeev, A. Forchel, Phys. Rev. B 71 (2005) 125335.
[10] H.-A. Engel, D. Loss, Science 309 (2005) 586.
[11] S.A. Crooker, J.A. Hollingsworth, S. Tretiak, V.I. Klimov, Phys. Rev. Lett. 89 (2002) 186802.
[12] X. Hu, T. Ritz, A. Damjanovic, F. Autenrieth, K. Schulten, Quarterly Rev. Biophys. 35 (2002) 1.
[13] C. Hettich, C. Schmitt, J. Zitzmann, S. Kuhn, I. Gerhardt, V. Sandoghdar, Science 298 (2002) 385.
[14] C.R. Kagn, C.B. Murray, M. Nirmal, M.G. Bawendi, Phys. Rev. Lett. 76 (1996) 1517.
[15] G. Vignale, M. Rasolt, Phys. Rev. Lett. 59 (1987) 2360.
[16] G. Vignale, M. Rasolt, Phys. Rev. B 37 (1988) 10685.
[17] H. Saarikoski, E. Räsänen, S. Siljämaki, A. Harju, M.J. Puska, R.M. Nieminen, Phys. Rev. B 67 (2003) 205327.
[18] E. Räsänen, A. Harju, M.J. Puska, R.M. Nieminen, Phys. Rev. B 69 (2004) 165309.
[19] H. Jiang, D. Ullmo, W. Yang, H.U. Baranger, Phys. Rev. B 69 (2004) 235326.
[20] E.A. de Andrada e Silva, G.C. La Rocca, F. Bassani, Phys. Rev. B 50 (1994) 8523.
[21] O. Voskoboynikov, C.P. Lee, O. Tretyak, Phys. Rev. B 63 (2001) 165306.
[22] Y. Li, J.-L. Liu, O. Voskoboynikov, C.P. Lee, S.M. Sze, Comput. Phys. Comm. 140 (2001) 399.
[23] J.I. Climente, J. Planelles, J.L. Movilla, Phys. Rev. B 70 (2004) 081301.
[24] W. Wang, T.-M. Hwang, W.-W. Lin, J.-L. Liu, J. Comp. Phys. 189 (2003) 579.
[25] T.-M. Hwang, W.-W. Lin, J.-L. Liu, W. Wang, Num. Lin. Alg. Appl. 12 (2005) 605.
[26] P. Hohenberg, W. Kohn, Phys. Rev. 136 (1964) B864.
[27] W. Kohn, L.J. Sham, Phys. Rev. 140 (1965) A1133.
[28] S.M. Reimann, M. Manninen, Rev. Modern Phys. 74 (2002) 1283.
[29] Y. Li, O. Voskoboynikov, C.P. Lee, S.M. Sze, Solid State Comm. 120 (2001) 79.
[30] G. Vignale, M. Rasolt, D.J.W. Geldart, Diamagnetic susceptibility of a dense electron gas, Phys. Rev. B 37 (1988) 2502.
[31] J.P. Perdew, Y. Wang, Phys. Rev. B 45 (1992) 13244.
[32] T.L. Beck, Rev. Modern Phys. 72 (2000) 1041.
[33] A. Stathopoulos, S. Öğüt, Y. Saad, J. Chelikowsky, H. Kim, Comput. Sci. Engrg. 3 (2000) 19.
[34] R. Barrett, M. Berry, T.F. Chan, J. Demmel, J. Donato, J. Dongarra, V. Eijkhout, R. Pozo, C. Romine, H. Van der Vorst, Templates for the Solution of Linear Systems: Building Blocks for Iterative Methods, second ed., SIAM, Philadelphia, 1994.
[35] M. Crouzeix, B. Philippe, M. Sadkane, SIAM J. Sci. Comput. 15 (1994) 62.
[36] G. Golub, C. van Loan, Matrix Computations, third ed., The Johns Hopkins University Press, 1996.
[37] C.-J. Huang, C.J. Umrigar, Phys. Rev. A 56 (1997) 290.
[38] C. Filippi, C.J. Umrigar, M. Taut, J. Chem. Phys. 100 (1994) 1290.